Review Article

A Review of Antenna Array Technologies for Point-to-Point and Point-to-Multipoint Wireless Communications at Millimeter-Wave Frequencies

G. Federico [iD],[1,2] **D. Caratelli** [iD],[1,2] **G. Theis** [iD],[1,2] **and A. B. Smolders** [iD][2]

[1]*Department of Research and Development, The Antenna Company, 5656 AE, Eindhoven, Netherlands*
[2]*Department of Electrical Engineering, Eindhoven University of Technology, 5600 MB, Eindhoven, Netherlands*

Correspondence should be addressed to G. Federico; g.federico@tue.nl

With the introduction of 5G communication systems operating in the mm-wave frequency range, new opportunities in terms of multimedia services and applications will become available. For this to happen, several technical challenges from an antenna standpoint need to be addressed. The achievements of high-gain characteristics and agile beamforming with wide-scan capabilities are the main targets of the ongoing research on mm-wave antenna arrays. In this paper, an up-to-date overview of antenna array technology for wireless communications at mm-wave frequencies is given. Particular focus is put on the review of the state-of-the art and most advanced antenna array concepts for point-to-point and point-to-multipoint radio links at said frequencies. Various figures of merit are assessed for a comprehensive analysis and bench marking of the technical solutions investigated in the presented survey.

1. Introduction

Wireless data traffic is exponentially increasing and such trend is expected to continue in the coming years. The capacity limit of wireless networks operating in the sub-6 GHz frequency band is effectively reached. As a matter of fact, most of the commercial radio-communication infrastructures, including AM/FM and high-definition TV broadcasting, as well as GPS, satellite, cellular, and Wi-Fi communications, are confined in relatively narrow portions of the spectrum between 300 MHz and 3 GHz where electromagnetic propagation conditions are more favorable, and low-cost semiconductor technology is readily available [1]. Said frequency range, however, is nowadays excessively crowded. For this reason, a significant effort has been put in place for the development of wireless communication systems operating at mm-wave frequencies, where larger bandwidth is available so to satisfy future capacity needs. The main advantages of communication systems operating at mm-waves can be summarized as follows [2]:

(i) Extremely wide bandwidths: compared to the frequency bands between 300 MHz and 3 GHz, mm-wave applications can benefit from wider portions of spectrum and, therefore, data rates.

(ii) Antenna size: the physical size of radiating elements decreases proportionally to the wavelength, allowing for integration of antennas and RF electronics to realize small form-factor devices.

(iii) Electromagnetic energy focusing: by virtue of the reduced operating wavelength, large-scale antenna arrays with more than 100 elements can be integrated into relatively small physical areas, allowing for adaptive beamforming to synthesize narrow beams with enhanced directivity characteristics which are instrumental to the delivery of better quality of service in real-life operative scenarios [3].

Wireless communications at mm-wave frequencies, however, also come with certain drawbacks, such as higher sensitivity to radio-wave blockage and larger propagation

losses. Furthermore, because of the specific quasioptical behavior of the electromagnetic field that dominates the physical layer, dedicated protocols in the MAC layer have to be developed [4] and adopted in order to achieve very low latency and high data rates [5]. At mm-waves, severe path losses are experienced in combination with a significant attenuation due to the impact of oxygen absorption (mainly in the 60 GHz band), blockage, precipitation, and foliage (associated with the presence of trees obstructing the radio link) [6]. However, several studies have confirmed that, for small distances (less than 1 km), rain attenuation has reduced impact on the distribution of the electromagnetic field radiated by small cells operating in the frequency range between 28 GHz and 38 GHz [7].

The unique characteristics of radio-wave propagation at mm-wave frequencies make the antenna one of the most critical elements in the overall system [8]. The higher level of antenna integration enabled by the higher frequencies of operation comes with the challenge of dealing with reduced tolerance to fabrication errors and more complex requirements for the materials employed. The antenna performance is obviously also affected by the characteristics of the circuitry embedded in the system, such as the feeding network to interconnect different components, or by the limitations in the active devices, like power and low-noise amplifiers. Another challenge in the design process at mm-waves is the characterization and testing of integrated antenna systems which, at such small wavelengths, are more sensitive to misalignment errors, temperature, and mechanical vibrations that, in turn, can result in additional losses, as well as amplitude and phase errors. More information on mm-wave antenna characterization can be found in [9], where a detailed analysis of measurement uncertainties at mm-wave frequencies is provided.

Many surveys and scientific papers concerning different aspects of the mm-wave technology have appeared in the literature during the last years. In [10], Wang et al. discussed the technical challenges faced in relation to phase noise and large-scale attenuation. In [11], Rappaport et al. provided an overview of the evolution of cellular and Wi-Fi networks with a detailed description of propagation channel models. In [12], Ghosh and Sen reported an inclusive survey on antenna array architectures. In [13], Hong et al. covered the aspects relevant to multibeam reflector-based array technology enabled by different phase-shifting techniques. Finally, in [14], Hong et al. described practical solutions for the integration of mm-wave phased-array antennas with beam-switching capabilities.

In this study, we focus on the review of different antenna array solutions classified according to the underlying technology. In particular, a detailed analysis of advanced arrays used for wireless communications at mm-wave frequencies is provided. Such an overview is, based on our knowledge, not published before in the open literature. The paper is organized as follows. In Section 2, useful design considerations are given together with some comments on the main challenges faced during the development of mm-wave array systems. Section 3 provides a description of the suitable antenna technologies employed at mm-wave

frequencies, highlighting the relevant advantages and disadvantages. In the subsequent sections, an extensive review is made of the state of the art of mm-wave antenna arrays for two specific use cases: point-to-multipoint (PtM) and point-to-point (PtP) wireless communications. Finally, concluding remarks are given in Section 7.

2. Design Considerations for MM-Wave Antennas

The next generation of wireless communication systems aims to support low latency and high data rates with extended coverage for a wide variety of applications, including sensor networks, smart buildings, and mobile devices [15]. The expression of the channel capacity is provided by the following equation [16]:

$$C = B \log_2 \left[1 + \left(\frac{\lambda_0}{4\pi r} \right)^2 G_{Tx} G_{Rx} \frac{P_t}{N_0} \right], \qquad (1)$$

which shows that the achievement of higher data rates is only possible by increasing the operational bandwidth (B) and the antenna gain at the transmit and/or receive ends (G_{Tx}, G_{Rx}) and by enhancing the signal-to-noise ratio (P_t/N_0). This explains the benefit associated with the use of the mm-wave spectrum, though at the cost of a larger free-space attenuation. In order to further improve the channel capacity, one can also enable multiple spatial data streams by supporting, concurrently, different beams and dual polarization at both the transmitter and receiver.

A key requirement of the antenna solutions for mm-wave communications is to feature high-gain characteristics so as to compensate for the significant propagation losses experienced at the considered frequencies. The solution to this challenge consists in the integration of antennas in array configuration [17], in combination with a sufficiently high density of deployment of cells in a given network. Upon increasing the number of radiating elements in an antenna array, one can increase directivity and thereby focus the radiated power in a given direction. The most common array structures are in rectangular/square configuration. A $M \times N$ planar array is shown in Figure 1, together with the coordinate system used as a reference in the rest of the document.

In order to achieve adequate radio coverage of the operating environment, it is imperative to perform an accurate link budget analysis. A key parameter in this respect is the path loss, which determines the level of attenuation of the radiated energy following the electromagnetic propagation process in the radio channel. Different models are available in the literature for the estimation of the path loss between transmitter and receiver. Of particular interest are the Close-In (CI) and the Alpha-Beta-Gamma (ABG) models which rely on experimental measurement data [18, 19]. An accurate evaluation of the link budget in Line-of-Sight (LOS) and Non-Line-of-Sight (NLOS) propagation scenarios for 5G-and-beyond communications is reported, also, in [20, 21] based on the 3GPP standard [22].

The main figures of merit that define the performance of an antenna array, as per the illustrations in Figure 2, are used
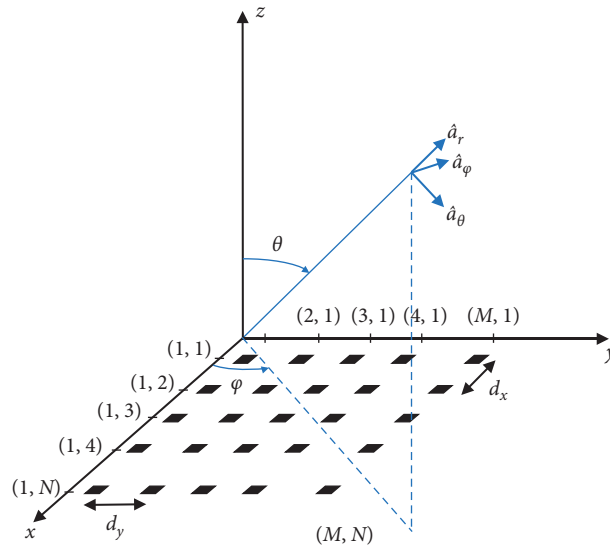
FIGURE 1: Schematic of a regular $M \times N$ planar array in a spherical coordinate system.
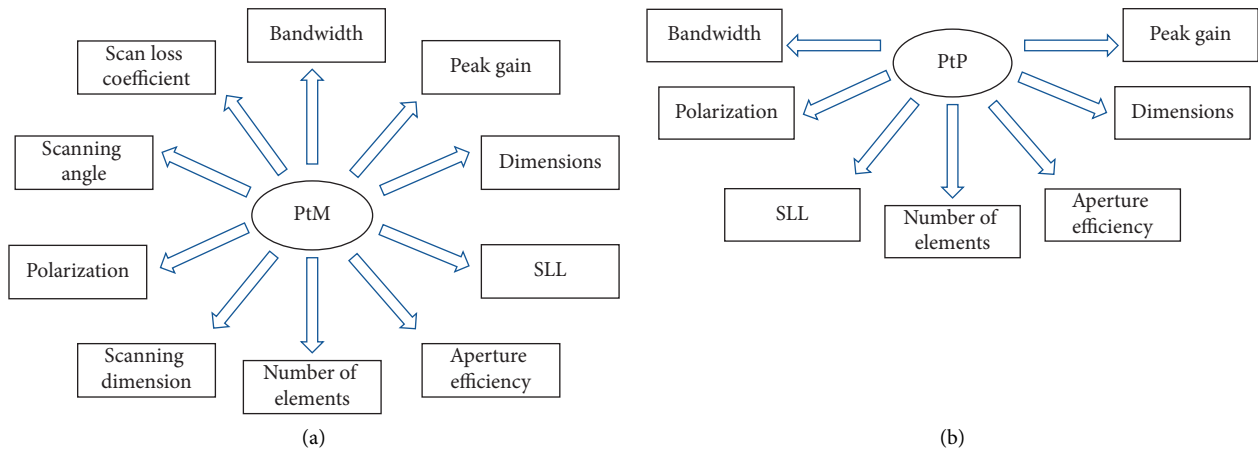

(a)

(b)

FIGURE 2: Figures of merit for the analysis of antenna arrays for (a) point-to-multipoint (PtM) communications and (b) point-to-point (PtP) communications.

in the following sections for bench marking of the technical solutions investigated in this review. For convenience, two different scenarios (PtP and PtM communications) have been examined in order to provide a more meaningful overview of the different antenna concepts considered here. Each operative scenario requires indeed different radiation characteristics.

When developing antenna arrays for PtP wireless communications, the main concern is to achieve high-gain characteristics in order to compensate for the propagation losses at mm-waves and obtain, in this way, a stable radio link while avoiding unexpected misalignment between the transmitter and receiver. Examples of PtP systems are found in midrange networks such as mm-wave backhaul/fronthaul as well as board-to-board communications. When an antenna array is used, instead, for PtM communications, one of the main challenges is to achieve wide-angle beam scanning. This allows minimizing the number of array antenna panels necessary to enable proper coverage of the operating

environment and, in this way, reducing the overall system costs. A relevant example in this respect is given by 5G base stations (BSs) that have to ensure a suitable 360° coverage of multiple users while they are in motion (as illustrated in Figure 3). In this case, in accordance with the aforementioned propagation loss models, one should target values of peak gain of about 26 dBi in order to enable a reliable quality of service up to 100 m in the frequency band at 28 GHz, as well as a scanning range of at least ±60° so to limit the required number of sectors to three or four (including some overlap margin). In this and several other operative scenarios, besides the wide-angle scanning capability, it is key to have antenna array solutions that feature stable gain and low Side-Lobe Level (SLL) characteristics. In addition to that, an important aspect to take into account during the design stage is the appearance of grating lobes. With reference to a uniformly spaced planar antenna array, the following criterion is typically enforced to avoid the formation of grating lobes [8]:
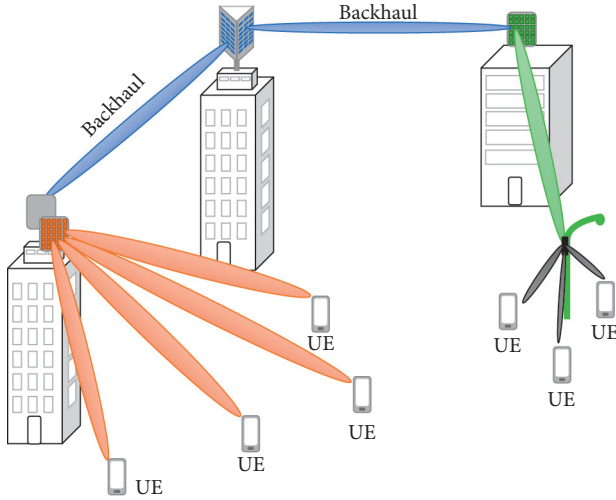
Figure 3: 5G wireless communication scenario where the use of PtP and PtM systems is shown in order to set up a communication system with user equipment (UE).

$$d_x, d_y < \frac{\lambda_0}{1 + \sin\theta_{\max}}, \tag{2}$$

where d_x and d_y denote the interelement separation along the horizontal and vertical directions, respectively, λ_0 is the wavelength in free space at the highest operational frequency, and θ_{max} is the maximal steering angle along each of the scan planes; that is, $\phi = 0°$ and $\phi = 90°$ (see also Figure 1). As it can be inferred from (2), grating lobes can be avoided by using a dense array grid. This can, however, cause unwanted high mutual coupling which, in turn, affects the array performance negatively. While scanning, broadside antenna arrays are subjected to a degradation of the mainlobe gain due to the aperture projection loss [23]. In ideal conditions, the gain degradation while scanning off boresight, also referred to as scan power loss, follows the $\cos\theta$ law. In real life, because of the impact of parasitic mutual coupling, scan loss is actually more severe and can be effectively modeled as $\cos^n\theta$, where n is a real-valued parameter larger than 1. The following considerations can be made [23]:

(i) The main-lobe gain decays at least as $\cos\theta$ while scanning in different directions.

(ii) A broadside array cannot scan up to the end-fire direction since $\cos(\pi/2) = 0$. Dedicated arrays should be designed to ensure end-fire coverage.

Grating lobes avoidance, high isolation between antenna elements, and stable gain over the scanning range are among the most relevant challenges and somehow conflicting requirements in the design of wide-angle scanning arrays.

An important figure of merit for antenna arrays is the active reflection coefficient (Γ_{A_m}), which provides an effective means for evaluating antenna return-loss characteristics inclusive of mutual coupling effects while scanning [24]. For the general m^{th} array element, Γ_{A_m} can be calculated as

$$\Gamma_{A_m} = \sum_{n=1}^{N} \frac{a_n}{a_m} S_{mn}, \quad m = 1, \ldots, N_a, \tag{3}$$

where N_a is the overall number of antenna elements, a_n and a_m denote the incident waves at the input terminals of the nth and m^{th} array element, respectively, and S_{mn} denotes the coupling coefficient. The operational bandwidth of a phased-array antenna is typically defined as the frequency range where the magnitude of the active reflection coefficient is below -10 dB. Blindness ($|\Gamma_{A_m}| \simeq 1$) may occur while scanning due to spurious coupling between antenna elements [24]. A detailed analysis of mutual coupling in phased arrays is provided in [25].

Among various aspects, the attainment of high efficiency over the entire frequency band of operation is important to enable effective power management at system level. With the billions of objects wirelessly connected to upcoming 5G communication networks, it becomes indeed crucial to reduce the power consumption of the individual devices and components.

3. Antenna Concepts and Technologies

The different antenna concepts available in the scientific literature offer a variety of design choices for array antennas which, with different characteristics, can strongly affect the overall system performance. An overview of the advantages and disadvantages of commonly used antenna elements integrated into mm-wave arrays is reported in Table 1.

Microstrip patch antennas are relatively easy to manufacture using technologies which are commonly available in industry [26]. They represent a quite versatile solution in several applications which require pencil beams, fan beams, or omnidirectional radio coverage. The antenna polarization, whether it is linear or circular, can be controlled in rather simple ways. Furthermore, microstrip antennas can conform to the shape of the hosting platform on flat or curved surfaces [27, 28]. Patch antennas are particularly suitable for PtM communications, since they feature a radiation pattern with broad coverage that is instrumental to the achievement of wide-angle scanning properties at array level.

Thanks to their characteristics, *Vivaldi antennas* [29] may represent a valid alternative to other antenna solutions in different applications. One of the main advantages of this type of antennas is the broadband behavior [30]. Vivaldi antennas are typically printed on dielectric substrates, thus making the relevant integration with other components of easier implementation. Vivaldi antennas have been extensively studied in literature with various design improvements [31, 32]. Many techniques have been developed to enhance the gain of this class of antennas, such as those based on the use of dielectric lenses [33–35], metamaterial lenses [36], and parasitic elliptical patches [37]. As Vivaldi antenna, end-fire radiation can also be realized with printed *dipole* or *bow-tie* antenna arrays, which have a similar built-up as shown in [38].

TABLE 1: Advantages and disadvantages of commonly used antenna technologies for array development.

Technology	Advantages	Disadvantages
Patch	(i) Integration (ii) Low cost	(i) Losses (ii) Isolation
Vivaldi	(i) Wideband (ii) High gain	(i) Bulky
DRA	(i) No conductor loss (ii) High efficiency	(i) Manufacturing precision
Open-ended waveguide	(i) Stable radiation pattern (ii) High efficiency	(i) Bulky (ii) High costs
Gap waveguide	(i) Low losses (ii) Wideband	(i) Design complexity
Resonant cavity	(i) High gain (ii) Low cost	(i) Narrow 3 dB gain bandwidth

Dielectric resonator antennas (DRAs) display excellent characteristics for high-frequency applications and in particular for mm-wave communications and remote sensing [39]. DRAs feature low losses, high efficiency, and wide bandwidth and can support multiple polarizations, as well as diverse radiation patterns by excitation of suitable resonant modes [40, 41]. The DRA size is proportional to $\lambda_0/\sqrt{\epsilon_r}$, which translates into the possibility of controlling the antenna dimensions by properly selecting the relative permittivity (ϵ_r) of the material forming the basic dielectric resonator. DRAs are easy to fabricate and enable good design flexibility based on different geometries. One of the main characteristics of DRAs is the absence of conduction losses, which makes them a very promising candidate for mm-wave applications [42]. Electrically large DRAs exploiting higher-order propagation modes are used to enhance antenna gain. At the same time, one should notice that the bandwidth is inversely proportional to the relative permittivity, and this may limit the choice of dielectric materials for a given application [43].

Thanks to high-gain and high-efficiency characteristics, *open-ended waveguide antennas* are largely employed in array configuration for mm-wave applications. This type of antennas, however, is not very attractive for commercial applications at mm-wave frequencies above 60 GHz because of the inherently high manufacturing costs, bulky dimensions, and less easy integration with a chip or in a package as compared to other technologies [15]. Nowadays, some of these limitations have been overcome thanks to the concept of *substrate-integrated waveguide* (SIW). The advantages of conventional waveguides are preserved with SIW structures. The SIW technology has recently replaced the conventional transmission lines in mm-wave communications due to favorable propagation characteristics, such as high-Q factor and high power handling capability [44]. The most important advantage of SIW technology is represented by the possibility of enabling full integration of all the system components on the same substrate [45]. Since SIW components are bounded by conducting surfaces on both sides of the substrate, they exhibit extremely low (completely negligible) spurious radiation losses and insensitivity to outer electromagnetic interferences (EMIs) [46]. *Gap-waveguides* are also presented in the technical literature as a possible solution for mm-wave wireless communications [47]. Gap-waveguide technology offers indeed good performance at mm-wave frequencies thanks to the relevant low-loss characteristics. Gap-waveguiding structures rely on the propagation of electromagnetic waves between two parallel metal plates, while the propagation direction is controlled through metal pins that do not have electrical contact with the lid that covers them [48]. The losses in gap-waveguides are comparable to the losses in conventional waveguides.

Resonant cavity antennas (RCAs) can also be a class of antennas to be considered for mm-wave applications. RCAs feature very high-gain characteristics with the drawback of a narrow gain bandwidth at 3 dB level. An extensive review of RCAs for 5G wireless communications is provided in [49].

4. Wide-Angle Scanning Antenna Arrays for PtM Communications

In this section, we provide an extensive review and comparison of the most common wide-angle scanning antenna array technologies available at mm-waves for PtM communications. The antenna array solutions considered here are detailed in Table 2 where the relevant figures of merit (see Figure 2(a)) are evaluated. The aperture efficiency (η_{eff}), as reported in Table 2, is calculated starting from the antenna gain characteristics through the following formula [50]:

$$\eta_{\text{eff}} = \frac{G\lambda_0^2}{4\pi A_{\text{phys}}},\qquad(4)$$

where G denotes the peak gain at the boresight and A_{phys} is the physical area of the antenna structure.

The scan loss of the relevant antenna arrays analyzed in this review is illustrated in Figures 4(a) and 4(b) along the azimuth plane and the elevation plane, respectively, and compared to the ideal case with $\cos \theta$ behavior. One can notice that the state-of-the-art solutions have scanning capabilities up to $\pm 60°$ but at the cost of at least 4 dB scan loss.

In [51], a 5G communication link at 28 GHz is demonstrated using a 64-element (8×8) phased-array consisting of stacked patch antennas. The design is based on four-channel (2×2) transmit/receive (TRX) beamforming chips in SiGe BiCMOS technology with 6-bit phase control.

TABLE 2: State of the art of antenna arrays for PtM mm-wave wireless communications.

Antenna technology	Bandwidth (GHz)	Peak gain (dBi)	Dimensions (mm²)	SLL (dB)	Aperture efficiency (%)	Number of elements	Dimension of beam scanning	Polarization	Max scan angle	Scan loss coefficient
Stacked patch [51]	28–32	22.5	50×63	−10	57	8×8	Azimuth and elevation	Single	Az.: ±50° El.: ±25°	Az.: $n = 1.5$ El.: NA
Patch on PCB [52]	26–31.4	12	23×23	−8	26	4×4	Azimuth	Dual	Az.: ±42°	Az.: $n = 2$
Dipole [56]	26.5–29.5	12	NA	−9	NA	8×1	Azimuth	Single	Az.: ±50°	Az.: $n = 2$
Patch [57]	57–66	21.5	14.1×22.4	−11	85	48	Azimuth and elevation	Single	Az.: ±60° El.: ±10°	Az.: $n = 1.7$ El.: NA
AiP patch/ dipole for UE [59]	28–29.5	14	NA	−7	NA	2×4	Azimuth and elevation	Dual	Az.: ±45° El.: ±45°	Az.: $n = 2$ el.: $n = 1.7$
AiP patch for UE [61]	27.5–29.5	14	11.6×22	−8	79	2×4	Azimuth	Dual	Az.: ±30°	Az.: $n = 1.7$
Patch for BS [62]	28–32	24	70×70	−9	47	8×8	Azimuth and elevation	Dual	Az.: ±50° El.: ±50°	Az.: $n = 2$ el.: $n = 1.5$
AiP patch [65]	80–100	30	45×45	−8	44	384	Azimuth and elevation	Dual	Az.: ±20° El.: ±30°	Az.: $n = 4.2$ El.: $n = 4.7$
Vivaldi for UE [66]	27.4–28.6	12	60×130	−10	30	1×8	Azimuth	Single	Az.: ±70°	Az.: $n = 0.5$
DRA for BS [68]	26–30	23.5	63.1×69.4	−12	44	8×8	Azimuth and elevation	Dual	Az.: ±60° El.: ±60°	Az.: $n = 1.5$ El.: $n = 1.5$
Gap waveguide [69]	26.5–31	24	135×122	−12	13	16×16	Azimuth and elevation	Dual	Az.: ±45° El.: ±10°	Az.: $n = 2$ El.: NA
Horn for BS [70]	26.5–29.5	24	50×50	−13	90	8×8	Azimuth	Single	Az.: ±45°	Az.: $n = 1.7$
FPA [77]	20–40	43	830×255	−12	80	200	Azimuth	Single	Az.: ±20°	NA

Sixteen chips are integrated on a 12-layer Printed Circuit Board (PCB) which includes a suitable Wilkinson power dividing/combining network. The antenna elements are spaced 5 mm (about $0.5\lambda_0$ at 30 GHz) apart in the horizontal direction and 6.3 mm (about $0.63\lambda_0$ at 30 GHz) apart in the vertical direction, as shown in Figure 5. The selected interelement spacing enables a maximal scan angle up to ±50° along the azimuth plane and up to ±25° along the elevation plane while achieving relatively low SLLs (below −10 dB) in combination with a peak gain of 22.5 dBi and a bandwidth of 4 GHz (from 28 GHz to 32 GHz). The antenna array is characterized by an Effective Isotropic Radiated Power (EIRP) of 50 dBm and is designed in such a way as not to require a dedicated calibration network. It has been tested and verified for radio links over a distance of up to 300 m.

A wideband patch antenna array that can support two linear orthogonal polarizations concurrently is presented in [52]. The antenna array is formed by 16 elements in a 4×4 configuration which is optimized so to operate in the frequency band between 26 GHz and 31.4 GHz. As known from theory, conventional rectangular or circular patch antennas typically feature a rather limited fractional bandwidth, up to about 7% [53]. In [52], a broader band of operation is achieved by realizing circular cutouts at the four corners of the basic square patch (see Figure 6). The individual radiating element has maximal dimensions of 2.65 mm × 2.65 mm, whereas the radius of the cutouts is

0.95 mm. The antenna element is excited by two feeding pins in order to support dual linear polarization. In the final 4×4 array configuration, the antenna elements are spaced 5.5 mm (about $0.57\lambda_0$ at 31.4 GHz) apart from each other along both the horizontal and vertical directions. The array beam-steering network is based on a Butler Matrix (BM) [54, 55], which is implemented on a circuit board with dimensions of 120 mm × 70 mm × 1.62 mm. The array is characterized by a maximal scan angle of ±42° and a peak gain level of 12 dBi.

A microstrip array dipole-based operating in the 28 GHz frequency band is detailed in [56]. A PTFE board of 15 printed dipoles is used to construct an array in a 15×8 configuration. The antenna elements are connected to the PCB through SMPM connectors and kept at a center-to-center distance of 6 mm. This supports a beam-scanning range beyond ±50° in the azimuth plane, in combination with a saturated EIRP of 39.8 dBm at the boresight.

A tile-based array for backhaul applications at 60 GHz has been presented in [57]. The unit cell consists of a slot-coupled microstrip patch that is parasitically loaded by four auxiliary patches (forming an H-shape). The position of the auxiliary patches has been chosen so to broaden the operational bandwidth while achieving an active reflection coefficient with magnitude below −10 dB in the frequency range between 57 GHz and 66 GHz. A tile with 48 unit cells is designed in a 6×8 array configuration. Measurements carried out on the individual tile have shown a peak gain of
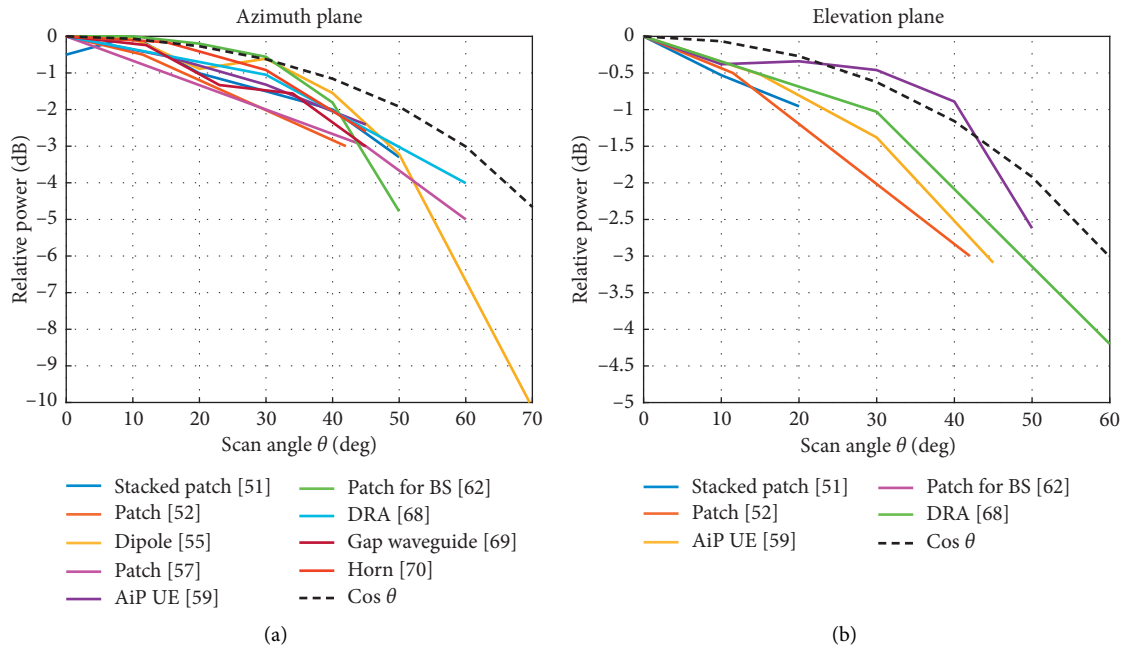
(a)

(b)

FIGURE 4: Scan loss of the most relevant antenna arrays along the azimuth plane (a) and the elevation plane (b).
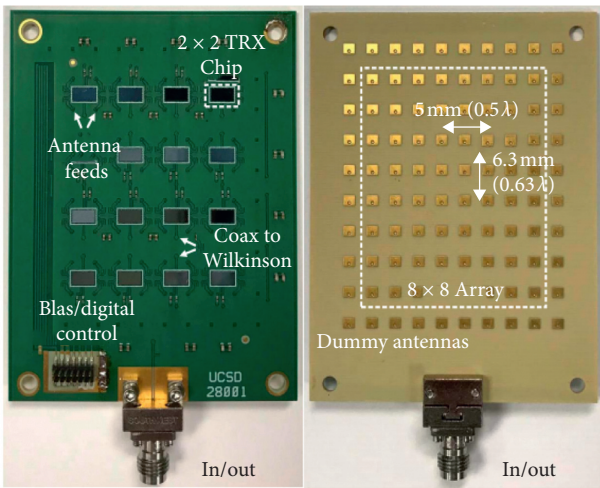

FIGURE 5: Top and bottom views of the 12-layer 64-element phased-array Printed Circuit Board (PCB) [51] ©2018 IEEE.

FIGURE 6: Patch element with angular circular cutouts of the 4×4 array configuration proposed in [52].

about 22 dBi at the boresight, which drops by 3 dB at ±45° and by 5 dBi at ±60° while scanning in the azimuth plane. When six of the aforementioned 48-element tiles are placed together in two rows to form a 288-element array, a peak gain of 29.5 dBi is achieved.

As documented in the previous section, microstrip antennas are particularly suitable for close integration with circuit components such as amplifiers and switches, so to realize an Antenna-in-Package (AiP) [58]. The need for AiP technology is going to increase dramatically for applications at mm-wave frequencies and beyond. AiPs are already being widely employed for 5G cellular network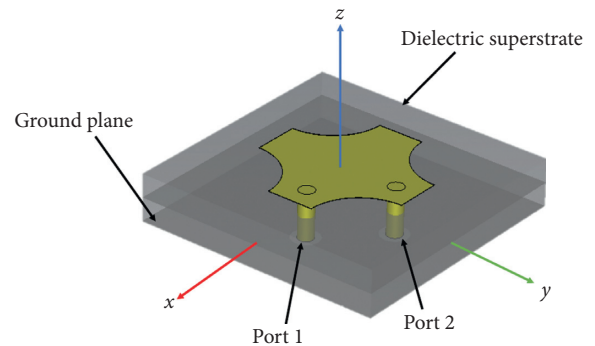 deployment at 28 GHz [59, 60]. In [59], a relevant phased-array transceiver with 24 channels and dual-polarization support is described. The UE module relies on different antenna array configurations, such as 1×4 dipole arrays and 2×4 patch arrays with integrated radio frequency integrated circuits (RFICs). The BS makes use of a 4×4 patch antenna array with 2 rows of dummy elements on one edge. Measurements carried out on the UE module with 2×4 integrated array have shown an uncalibrated scan range up to ±45° for both the horizontal and vertical polarization channels along the azimuth plane, whereas the achieved peak EIRP level is 35 dBm for horizontal polarization and 34 dBm for vertical polarization.

A similar dual-polarized design for UE (see Figure 7) is proposed in [61]. The relevant 2×4 patch antenna array with dual feeds is integrated into a Flip Chip-Chip Scale Package (FC-CSP) with a relative permittivity of 3.9 and 8 metal layers having a thickness of 800 μm and a total area of 11.6 mm × 22 mm. The separation between antenna

elements is equal to 5.25 mm (i.e., $\lambda_0/2$ at the center frequency of 28.5 GHz). The individual antenna element occupies an area of 2.35 mm × 2.35 mm and features an average peak gain of 5 dBi when integrated into an array configuration. The complete array displays a peak gain along the broadside direction of about 14 dBi with a scan range of ±30° along the azimuth plane. In the frequency band between 27.5 GHz and 29.5 GHz, the maximum EIRP of the considered array is 31.5 dBm.

An antenna module operating at 28 GHz is proposed in [62] and is shown in Figure 8. In this design, the multilayered phased-array antenna consists of 64 dual-polarized active patch antennas and 36 dummy elements. The dummy elements are placed along the periphery of the array, whereas the active elements are fed by 4 RFICs. An air cavity is implemented underneath all the array elements to improve bandwidth and, at the same time, suppress spurious antenna coupling processes. The measured peak gain of the individual antenna element is about 7 dBi at 30.5 GHz. The array is claimed to scan from −50° to ±50° and features an EIRP larger than 50 dBm. The module has a size of 70 mm × 70 mm with a thickness of 2.3 mm.

AiP technology is being broadly employed, also, for smart sensing and short-range wireless communications in the 60 GHz band. An example of this is reported in [63], where a package that integrates 6 patch antennas is designed in such a way so as to deliver a combined gain of about 10 dBi. Thanks to the very compact dimensions, namely, 14 mm × 14 mm × 0.8 mm, the aforementioned AiP has the potential of being integrated into a wide range of wearable devices [64].

The use of W-band technology for 5G applications has been investigated in [65] using a scalable tile-based phased-array architecture. The individual tile consists of a 5 × 5 aperture-stacked patch antenna array which is partitioned into 16-element and 8-element subarrays, in addition to a dummy element. The antenna spacing is selected to be $0.63\lambda_0$ at 90 GHz (i.e., 2.1 mm) along both the vertical and horizontal directions. In order to avoid grating lobes while scanning, it is advisable to keep the array elements at a separation smaller than or equal to $0.5\lambda_0$. However, such layout could not be implemented in [65] because of the physical constraints set by the adopted RFIC solution as well as by the limitations of the adopted PCB manufacturing process. The developed single tile covers the frequency range from 80 GHz to 100 GHz, with simulated directivity, gain, and efficiency better than 18.5 dBi, 18 dBi, and 87%, respectively. The integration of 16 array tiles results in a total EIRP level of 60 dBm and a beamwidth of less than 4° at 90.7 GHz. The 2D beam-steering function can be achieved by integrating any number of tiles.

Vivaldi antenna arrays have been proposed for 5G mobile terminals in [66]. The design consists of 8 antenna elements integrated along the edge of the device PCB and optimized in such a way so as to feature a central working frequency of 28 GHz with an operational bandwidth larger than 1 GHz. The array is characterized by a scan range up to ±70° with a total efficiency of more than 84%. The peak gain of the array beam is shown to be nearly flat around 12 dBi over the scan range from the boresight to ±40°.
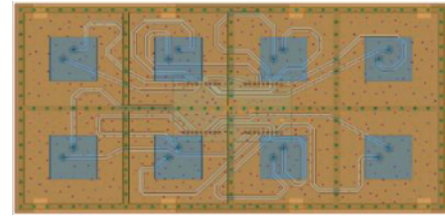

Figure 7: Antenna array for UE proposed in [61] ©2017 IEEE.

Another interesting solution for wide-angle scanning arrays is represented by DRA technology. The introduction of DRAs in literature dates back to 1983 when Long et al. presented the first detailed mode analysis of resonant cylindrical dielectric cavities in [67]. After that, DRAs have been used in a variety of applications over a wide frequency range, from 55 MHz up to 340 GHz [43]. A relevant study concerning the application of DRA technology in mm-wave antenna arrays for 5G applications is proposed in [68]. The array demonstrator discussed in the said study is shown in Figure 9. Each parallelepipedal DRA element forming the array structure is fed by a slot aperture which, in turn, is excited by proximity coupling through a dedicated microstrip line. The array elements are placed along a uniformly spaced 8 × 8 grid on the top of a feeding network integrated into a PCB with an overall size of 63 mm × 69 mm. It is shown that a total efficiency larger than 80% is achieved in the frequency band from 28 GHz to 30 GHz in combination with a maximal scan range of ±60° along both the azimuth and elevation planes. The realized gain displayed by the array along the broadside direction is about 23 dBi at 28 GHz, with a minimum level of 21.5 dBi across the frequency range from 24 GHz to 30 GHz.

A relevant design solution for 5G BSs based on gap-waveguide technology is presented in [69]. In this research, a slotted-waveguide array antenna is implemented by means of a fully integrated all-metal multilayered assembly. Waveguide-like feeding lines are realized using artificial magnetic conductors, without the need for electrical connections between the layers forming the array structure. This enables the integration with substrate-based components. The radiating antenna layer consists of an 8 × 8 array of slots and is characterized by an active reflection coefficient with a magnitude below −10 dB in the wide frequency range from 26.5 GHz to 31 GHz. The array features a peak main-lobe gain of 23 dBi with a maximum scan range of ±45° along the azimuth plane and ±10° along the elevation plane.

In [70], a phased-array based on compact horn antennas is proposed. Such an array is optimized for operation in the 26.5 GHz–29.5 GHz frequency band. A 2 × 2 subarray is used as a building block to realize a scalable $M \times N$ array. In the subarray, the feed of each radiating element is at a distance of 5.84 mm from the neighboring elements along both the vertical and horizontal directions. The numerical simulation results of the 4 × 4 array, as illustrated in Figure 10, show a scanning capability of ±45° along the azimuth plane with a peak gain ranging from 21.48 dBi to 23.99 dBi. The array has been scaled up to 8 × 8 array elements and in this case, the main-lobe gain level is comprised between 27.81 dBi and 29.99 dBi.

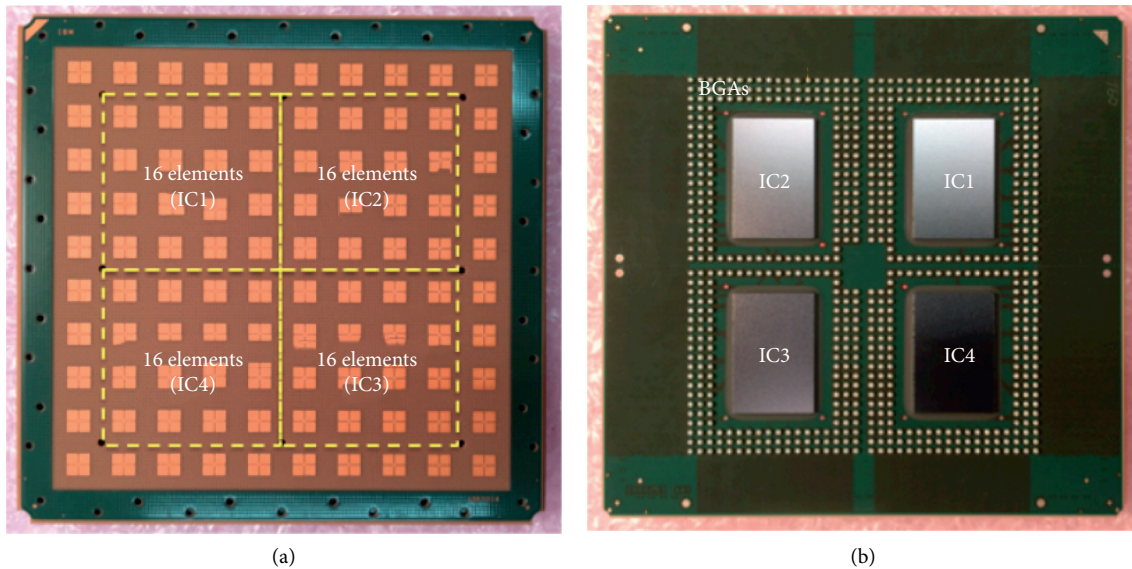(a)   (b)

FIGURE 8: Top view (a) and bottom view (b) of the antenna module as presented in [62] ©2019 IEEE.

FIGURE 9: Top view of the 8×8 DRA array proposed in [68].

In [71] a multimode horn antenna is used, instead, in a linear array configuration with sparse topology. The size of the individual radiating element is $2.0\lambda_0 \times 1.8\lambda_0$ at 28.5 GHz. This results in a peak gain of 11.5 dBi in combination with a 120° scanning range along the azimuth plane of the array. It is shown that the irregular sparse array can improve the system performance by decreasing the outage probability (referring to the probability that the Carrier to Noise Ratio is lower than 3 dB).

An alternative to horn and gap-waveguide technologies is represented by the use of open-ended waveguide arrays. The design presented in [72] is capable of scanning up to ±60° along both principal planes. A drawback of such technology, however, is the significantly more complicated manufacturing process. Furthermore, the integration of such radiating structures with printed circuits and components is not mature yet and requires additional research.

The design concepts presented up to now make use of phase shifters and variable gain amplifiers for each antenna element in order to realize beamforming. This requires the use of multiple power-hungry ICs. In [73, 74], an alternative solution is presented, where the use of a lens is investigated as a replacement to said ICs. The lens-based array antenna reported in [75] is

optimized for 5G PtM wireless communications at mm-wave frequencies. The prototype is shown in Figure 11. The basic radiating structure is formed by a standard 4×4 patch antenna array with a size of 55 mm × 55 mm. The size of the individual patch antenna is 3.05 mm × 3.05 mm with an interelement spacing of λ_0 at the frequency of 30 GHz. The design relies on a hyperbolic dielectric lens made out of polyethylene, with a diameter of 155 mm. The concept is based on the independent control of the individual patch antennas so to focus the radiation beam in different directions according to a suitable beam-switching scheme. The working frequency band of the radiating structure is rather narrow and is limited to the range from 27.8 GHz to 28.4 GHz. The peak gain achieved with the considered design is about 12.12 dBi with an improvement of about 8 dBi as compared to the same radiating structure without integrated dielectric lens. The maximum scan range is about 15° but, as mentioned in [75], this can be further improved by using higher-order patch antenna array configurations.

Another alternative hybrid beamforming concept is represented by focal-plane arrays (FPAs) [76, 77]. Similar to the use of lens antennas, they provide a more limited scan range, which makes these concepts, in general, less suited for PtM applications.

5. High-Gain Array Antenna-Based Concepts for PtP Communications

In this section, we provide an overview of available antenna array concepts and technologies for mm-wave PtP communications. For such applications, key design aspects are the antenna beamwidth and directivity. These need to be carefully optimized to prevent system performance failure due to unwanted misalignment. Most of the PtP radio links are in fact designed for LOS communications in outdoor scenarios where devices are exposed to weather and environmental factors which can cause degradation of the quality of service (QoS). Reflectors, lens or DRAs, FPAs, and
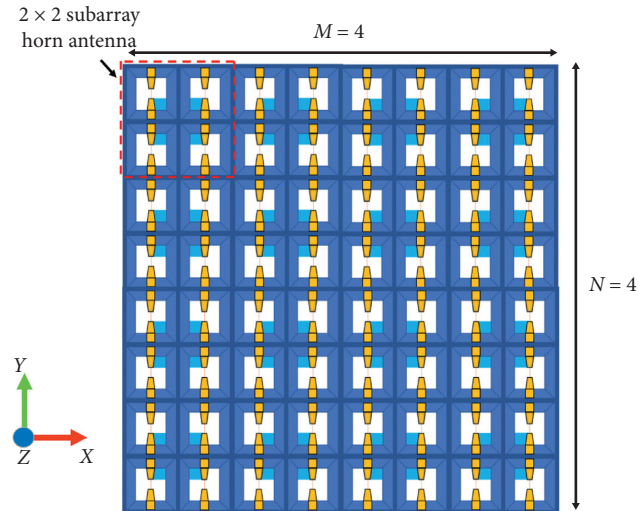
FIGURE 10: Top view of a 4×4 horn-based array antenna as presented in [70].
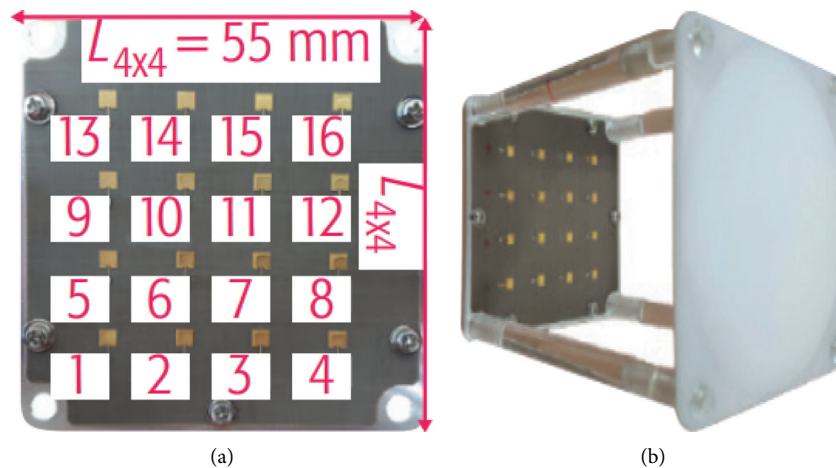

| (a) | (b) |

FIGURE 11: Patch array (a) and lens antenna array prototype (b) proposed in [75] ©2018 IEEE.

reflectarrays are usually preferred to other classes of radiating structures for PtP communications by virtue of the high-gain characteristics they display. Alternative antenna technologies can, however, provide solutions in specific operative scenarios and are often employed [8]. The antenna concepts for mm-wave PtP communications reviewed in this study are illustrated in Table 3.

Thanks to the relevant high-gain characteristics, reflectarrays are becoming appealing for 5G applications. The solution proposed in [78] is a reflectarray based on microstrip patch antennas. The array operates in two frequency bands (around 27 GHz and 32 GHz) by integration of two sets of radiating elements which cover each band, separately. A horn antenna is used as a feeding structure. As mentioned by the authors, the considered reflectarray is not optimized in terms of bandwidth, and information in this respect is not made available. The design is optimized to support dual polarization. Such performance is achieved by properly rotating the radiating elements by 90°. The 2×2 patch assembly that constitutes the subarray cell has an overall size of 5.5 mm × 5.5 mm (which is $0.58\lambda_0$ at 32 GHz). The reflection phase is corrected for each frequency band/polarization by independently tuning the dimensions of each element. The total size of the reflectarray based on a 15×15 subarray configuration is approximately 82.5 mm × 82.5 mm. A peak gain of 27.5 dBi is observed at 32 GHz. Because of the relatively small dimensions, the design is affected by high spillover losses which result in an aperture efficiency of 29% at 27 GHz and 38% at 32 GHz.

The reflectarray proposed in [79] for operation in the frequency range from 30 GHz to 40 GHz is instead based on the use of DRA elements. The unit cell has a circular shape with four arms, and the relevant radius is tuned in a suitable way when moving from the center to the edge of the reflectarray so to synthesize the required reflection phase response. The unit cells embedded in the structure are 446, arranged in a circular array with a maximal radius of 60 mm. A horn antenna is used as a feeder. The choice of DRAs as

TABLE 3: State of the art of high-gain array-based antenna concepts for PtP mm-wave wireless communications.

Antenna technology	Bandwidth (GHz)	Peak gain (dBi)	Dimensions (mm^2)	SLL (dB)	Aperture efficiency (%)	Number of elements	Polarization
AiP patch [63]	57–64	10	14×14	−7.5	11	2×2	Single
Lens antenna [75]	27.8–28.4	25	100×100	−8	30	2×2	Single
Patch reflectarray [78]	NA	27.5	82.5×82.5	−12	38	15×15	Dual
DRA reflectarray [79]	30–40	24.8	$60 \times 60 \times \pi$	−10	26	446	Single
Double-ring reflectarray [80]	26–35	37.8	$177 \times 177 \times \pi$	−14	60	NA	Single
DRA [81]	29–34.3	16.29	NA	−10	NA	4×4	Circular
GDRA [83]	29.3–35.2	12	36.5×8	−10	38	1×8	Single
GDRA [84]	55–62	19.4	23×20	−14	38	8×8	Single
3D printed horn [85]	27.6–38.1	33.8	140×140	−15	86	16×16	Single
Vivaldi [86]	28–38	24.1	97.5×42	−7.7	32	4×4	Single
SIW horn [88]	25.25–32.6	17.2	70×2.8	−12	80	1×4	Single
SIW horn with lens [89]	26.7–27.3	15.65	112×2.5	−9.63	63	1×8	Single
SIW stacked patch [90]	25–33.7	20.3	100×90	−9	20	4×4	Circular
Slotted waveguide [91]	71–81	39.4	210×220	−18.9	24	512	Single
Gap waveguide [92]	57–66	33.3	80×80	−12	64	256	Single
Resonant cavity [93]	26–31.3	14.1	19×19	NA	65	2×2	Circular

basic radiating elements allows removing conductor losses and, in this way, attaining a measurably high peak gain of 23.9 dBi at 34 GHz and of 24.8 dBi at 35 GHz.

In [80], a reflectarray with very high-gain characteristics over a wide frequency range is presented. The design approach adopted for this purpose is based on a spatial dispersion compensation concept. The reflectarray is formed by a single-layer printed structure consisting of patch and double-ring (multiresonant) elements with properly selected dimensions, arranged according to a circular array scheme. The array has a maximal radius of 350 mm and is divided into two areas: the first area, closer to the center, is formed by double-ring elements, whereas the second area, towards the edge, is formed by patch elements. The frequency-phase response of each element can, in this way, compensate for the dispersion process caused by different propagation paths. The considered reflectarray is characterized by peak gain up to 37.8 dBi at 34 GHz, with a minimum level of 36 dBi across the entire operational frequency band from 26 GHz to 35 GHz.

As mentioned above, lenses are often employed for PtP wireless communications, thanks to their capability of drastically enhancing the antenna gain. The design presented in [75] demonstrates this once more. A conventional patch antenna is used as a basic radiating element with a peak gain of about 6 dBi. Thanks to the integration of a suitable cubic lens, the gain level is increased up to 12 dBi. The dimensions of the individual antenna, inclusive of lens, are $50 \text{ mm} \times 50 \text{ mm} \times 60 \text{ mm}$. The radiating element can be easily arranged in a linear or planar array configuration. Measurements of the 1×4 array and 2×2 array have shown a peak gain of approximately 25 dBi at 28 GHz.

In [81], a circularly polarized dielectric resonator antenna array for mm-wave frequencies is presented. In order to achieve circular polarization, X-shaped slots are etched off the ground plane so to excite the radiating elements while removing the need for more complex pin probes. In order to

enhance the bandwidth of the array, a sequential feeding network is used, similarly to the design concept illustrated in [82]. The simulated impedance bandwidth extends from 24.1 GHz to 31.1 GHz, whereas the simulated axial ratio (AR) bandwidth at 3 dB level extends from 26.9 GHz to 33.7 GHz. The antenna structure realizes, at the working frequency of 30 GHz, a peak gain of 12.44 dBi when arranged in a 2×2 array scheme and of 16.29 dBi in a 4×4 configuration.

An attractive alternative solution to conventional dielectric resonator arrays for mm-wave applications is reported in [83]. Here, an artificial grid dielectric resonator antenna (GDRA) is optimized in such a way so as to deliver high gain in combination with wideband characteristics at mm-wave frequencies. The size of the individual GDRA is only $2.7 \text{ mm} \times 2.7 \text{ mm} \times 0.5 \text{ mm}$ (i.e., $0.29\lambda_0 \times 0.29\lambda_0 \times 0.05\lambda_0$ at 32.2 GHz). Each GDRA is bonded to the substrate and is excited through a slot whose length is chosen to be approximately $\lambda_{\text{eff}}/2$, with λ_{eff} denoting the effective wavelength. The slot is realized in a SIW channel in combination with a suitable transition in microstrip technology. The GDRA elements are arranged in 1×4 or 1×8 array configurations, as illustrated in Figure 12. The eight-element array shows an impedance bandwidth at 10 dB return-loss level of 5.3 GHz (i.e., from 29 GHz to 34.3 GHz) with an improvement of 2.65 GHz as compared to the four-element array. The peak realized gain of the eight-element array is 12.13 dBi against 10.2 dBi featured by the smaller configuration. An efficiency level above 85% across the relevant operational frequency band is reported for both arrays. The same design solution can be tailored for applications at 60 GHz as documented in [84]. Here, GDRAs have been characterized in 4×4 and 8×8 array configurations. The operational band is from 56.5 GHz to 63 GHz in the former case and from 55 GHz to 62 GHz in the latter case. Experimental measurements carried out on the 4×4 and 8×8 GDRA arrays have shown a peak gain of 15.2 dBi and 19.4 dBi, respectively. According to the authors, the

proposed solution offers a lower profile and much wider impedance bandwidth as compared to conventional DRAs.

A 3D printed horn antenna array is investigated in [85]. Using such radiating element, a 16×16 array including a full-corporate air-filled waveguide network is designed for operation in Ka-band. The overall footprint size of the considered array is approximately $14\,cm \times 14\,cm$. The maximum broadside gain is 33.8 dBi, whereas the impedance bandwidth at 10 dB return-loss level is from 28.2 GHz to 35.8 GHz. The radiation efficiency is reported to be about 85% at the center of the operating frequency band.

In [86], a 4×4 array of slot-coupled Vivaldi antennas (SCVAs) is presented. The structure is optimized for 5G wireless communications and is demonstrated to have a wide impedance bandwidth, from 25 GHz to 40 GHz, in combination with high-gain characteristics. As a matter of fact, the individual SCVA features a peak gain of 13 dBi. On the other hand, the 4×4 array (see Figure 13) shows a broadside gain of 22.3 dBi at 28 GHz and 24.1 dBi at 38 GHz.

SIW technology is often adopted to ease fabrication and integration of horn antennas operating at mm-wave frequencies [87–89]. A relevant example of that can be found in [88], where a 1×4 array of hollow SIW (HSIW) H-plane horn antennas are realized using conventional, inexpensive though lossy, FR4 laminates. Under such assumption, HSIW technology provides an effective means for avoiding/reducing dielectric losses. The size of the individual horn antenna element is $18\,mm \times 25\,mm \times 2.8\,mm$, while a long dielectric load is used to improve the impedance matching characteristics, as shown in Figure 14. It is claimed that the radiating structure features an efficiency of 66.5% over the working frequency band from 27.6 GHz to 38.1 GHz, in combination with a maximum realized gain of 17.2 dBi.

Different methods have been introduced in the literature to improve gain and impedance matching properties of SIW-based horn antennas. In [87], a perforated dielectric slab is used to properly load the horn, whereas in [89], the horn antenna gain is boosted using an elliptical dielectric lens.

In [90], a novel SIW-based feeding network is cooptimized with a coplanar waveguide (CPW) fed array in such a way so as to achieve a wide bandwidth in terms of AR for applications in Ka-band. The basic radiating elements used in the considered design are stacked microstrip antennas. The array is formed by 4×4 subarrays, with each subarray consisting of 4×4 stacked patches. The relevant driven patches are embedded in the middle layer as shown in Figure 15. The overall size of the array is $106\,mm \times 90\,mm \times 1.016\,mm$. The radiation pattern features strong grating lobes since the distance between adjacent driven patches is $1.35\lambda_0$. Measurements show a bandwidth at 2 dB AR level from 25.25 GHz to 32.6 GHz in combination with a peak gain of 20.32 dBi at 30.5 GHz.

For fixed beam applications, slotted waveguides represent a sounding solution thanks to their high-gain and high-efficiency characteristics. The array proposed in [91] is a 32×64 slot array antenna with unequal beamwidths in the relevant horizontal and vertical planes. Measurement results show a return loss above 14 dB in the entire frequency band from 71 GHz to 81 GHz and a peak gain level of 39.4 dBi. The
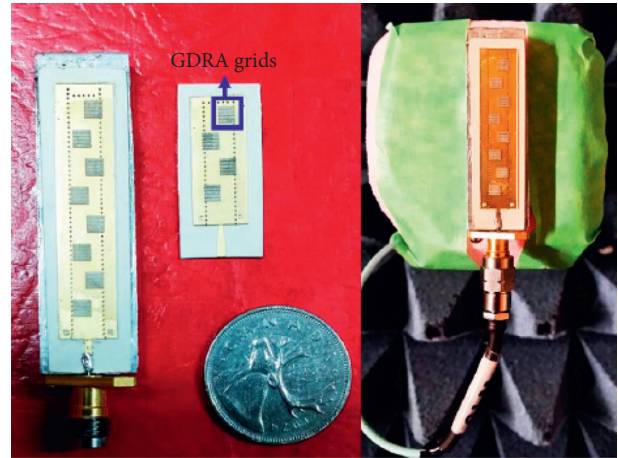

FIGURE 12: Illustration of the 1×8 (on the left) and 1×4 (on the right) GDRA arrays realized in [83] ©2019 IEEE.
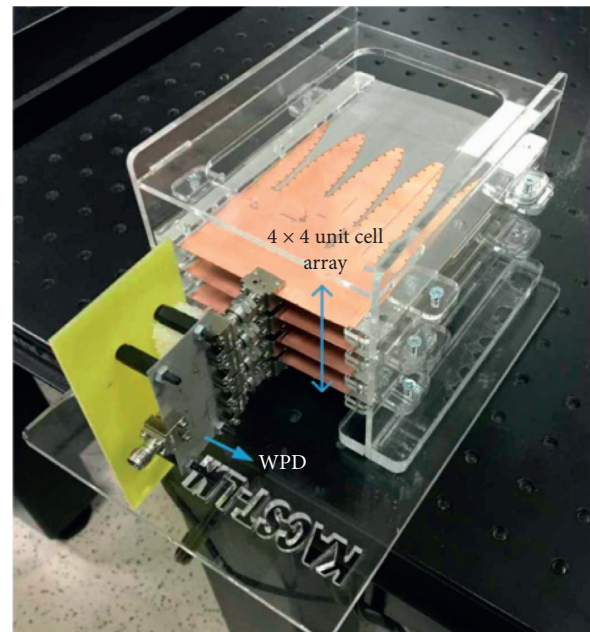

FIGURE 13: Box for placement of the four 1×4 antenna arrays as shown in [86].

design presented in [92] is, instead, a high-gain slotted antenna array based on gap-waveguide technology. The antenna elements are designed using groove ridge and inverted microstrip solutions. The array consists of 16×16 radiating slots which cover the frequency band from 57 GHz to 66 GHz, with a peak gain of about 33.3 dBi at the center of the band in combination with an SLL below −12 dB.

As mentioned in Section 3, a high antenna gain can also be achieved by means of RCAs. As an example, the 2×2 array described in [93] relies on a Fabry-Perot resonant antenna structure. The individual array elements consist of a corner-cut patch with a diagonal slot, and each antenna is sequentially rotated by 90° in order to improve the relevant isolation. The considered array is characterized by a broad 3 dB AR bandwidth that ranges from
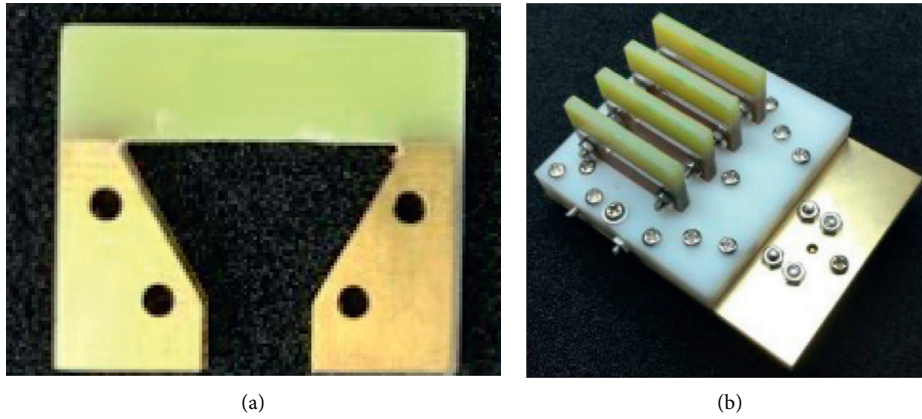
(a)

(b)

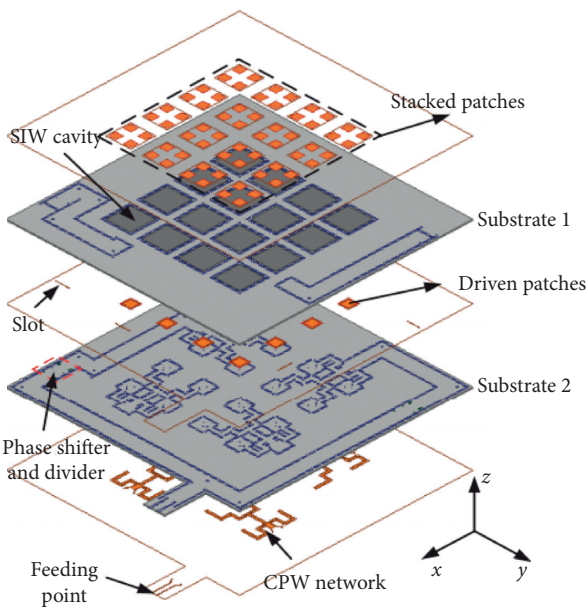FIGURE 14: HSIW Horn antenna element (a) and antenna array (b) proposed in [88] ©2019 IEEE.

FIGURE 15: Layer configuration of the antenna array in [90] ©2018 IEEE.

FIGURE 16: Aperture efficiency on the left axis and relative bandwidth on the right axis.

26 GHz to 31.3 GHz, in combination with a peak gain of 14.1 dBi at 28 GHz.

In Figure 16, the aperture efficiency, as computed by (4), and the relative bandwidth of each design concept for mm-wave PtP communications analyzed in this section are illustrated. One can notice how antenna arrays manufactured in waveguide/gap-waveguide technology tend to feature high aperture efficiency and wide bandwidth. As discussed in the previous sections, such benefit comes at the expense of significantly larger complexity and more expensive manufacturing process. Furthermore, this technology does not lend itself to the support of dual-polarization characteristics as it is now typically required for antenna systems for 5G communications.

Next to the overview in Table 3, it is important to stress that several research groups have developed alternative design approaches for gain enhancement of array antennas [94–99]. In [98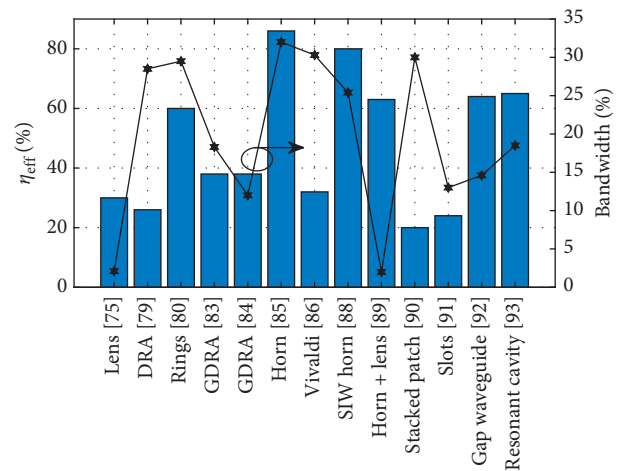], a straight slot is transversely introduced at the center of a patch. The slot acts as a secondary radiator which contributes to the enhancement of the antenna gain by about 1.7 dB without increasing the patch size. In [99], electromagnetic band-gap (EBG) structures have been employed to improve the gain of a 2×2 patch array antenna operating at 60 GHz. The merit of EBG structures is to suppress TM-mode surface waves [99], resulting in a gain enhancement of about 4 dB. On the other hand, the design solution illustrated in [97] enables a measurable gain increase thanks to the integration of a dielectric superstrate with circular holes. In combination with a 2×2 square patch antenna array, the use of the aforementioned superstrate structure results in a wider bandwidth of 15.35% and a nearly flat gain of 16 dBi in the frequency range from 26.5 GHz to 30.8 GHz.

6. Analysis and Discussion

The state-of-the-art overview provided in the previous sections gives a flavor of the wide variety of existing antenna concepts available in the literature; each of them characterized by different performance, benefits, and limitations. For mm-wave applications, ease of fabrication and a high

level of integration are key. It is not uncommon that a specific antenna technology is chosen mainly on the basis of manufacturing costs and integration constraints even if that results in largely suboptimal RF characteristics such as gain, efficiency, and bandwidth. The radiation properties of a given antenna element are also an important factor in the technology selection process. Broadside antennas are usually easier to integrate into array configuration, while end-fire radiating elements are most amenable for edge integration. To date, microstrip patch antennas are among the most used radiating elements for mm-wave arrays, although microstrip technology severely suffers from material losses and performance limitations at said frequencies.

One of the design challenges at mm-waves is associated with the correct knowledge of the material properties. At shorter wavelengths, it is certainly not straightforward to characterize dielectric materials with high accuracy. Furthermore, manufacturers typically provide, in their datasheets, detailed information regarding the complex permittivity of their own materials only up to 10 GHz. This is a definitive gap and possible drawback since even secondary materials such as soldermask may lead to unforeseen losses at the considered frequencies when neglected [100].

The main two types of losses at mm-wave frequencies are conductor and dielectric losses, with the former being typically more severe than the latter. The conductor losses quickly increase with frequency, due to the skin effect. The skin depth quantifies how close to the surface of a given conductor the electric current flows [101]. When the skin depth is approximately equal to the roughness of the conductor, a significant impact on the current flow is noticed. In fact, under said conditions, the surface roughness causes an increase of the parasitic inductance and, in turn, of the insertion loss [102]. Conductors with high melting temperature, low resistivity, low surface roughness levels, and good solderability are to be preferred for high-frequency circuit design [103]. The most common conductors with said characteristics are copper, gold, silver, aluminum, and palladium-silver alloys [103].

At mm-wave frequencies, the assumption of electrically thin dielectric substrates may be not valid any longer [104]. In the presence of thick substrates, surface wave modes are excited removing, in this way, power from the main beam radiation process; because of that, they can be regarded as a loss mechanism [12].

The choice of materials for mm-wave antenna array design is also related to another important challenge, that is, the thermal management. A growing number of research studies is being devoted to this problem [105], and highly efficient antennas are important to reduce the ohmic losses which contribute to the overall power dissipation budget. In this perspective, as seen in the previous sections, DRA and waveguide arrays showed good performance at mm-waves thanks to the high-efficiency and low-loss characteristics which they exhibit.

7. Conclusions

In this paper, an extensive overview of the state of the art of the most recent antenna array solutions for mm-wave communications has been given. In the first part of the manuscript, the development challenges at mm-wave frequencies have been discussed with particular focus on the antenna integration aspects associated with miniaturization, as well as the constraints relevant to the channel propagation characteristics and the need for cost and energy-efficient system design. In the subsequent sections, the recent developments in antenna technology for high-frequency applications have been surveyed, while highlighting the advantages and disadvantages of the most relevant designs available in the scientific and technical literature. In order to provide the reader with a rational classification, two different use cases have been identified: PtM and PtP wireless communications. The former requires the use of wide-scanning arrays, whereas the latter relies on high-gain directional antenna technologies.

For the first use case scenario, patch antenna arrays are widely used thanks to the radiation characteristics, which allow wide-angle scanning on both relevant planes. At the same time, DRA solutions are also emerging as promising candidates in this respect. For the second use case scenario, instead, reflectarrays, FPAs, and lens or dielectric resonators are preferred to other array technologies. In both cases, integration and manufacturability are key aspects in the selection of suitable antenna technology, while dedicated design approaches have to be adopted in such a way so as to ensure optimal scanning performance with stable gain, low-losses, and high-efficiency characteristics.

In the future, important opportunities will be offered by the advent of 6G communication systems as broader frequency bands will become available at even higher frequencies. At the same time, new challenges will have to be addressed, such as those associated with progressively higher propagation losses and tighter integration between electronic circuitry and antenna subsystems.

Conflicts of Interest

The authors declare that they have no conflicts of interest.

Acknowledgments

References

[1] Z. Pi and F. Khan, "An introduction to millimeter-wave mobile broadband systems," *IEEE Communications Magazine*, vol. 49, no. 6, pp. 101–107, 2011.

[2] X. Wang, L. Kong, F. Kong et al., "Millimeter wave communication: a comprehensive survey," *IEEE Communications Surveys & Tutorials*, vol. 20, no. 3, pp. 1616–1653, 2018.

[3] A. Naqvi and S. Lim, "Review of recent phased arrays for millimeter-wave wireless communication," *Sensors*, vol. 18, no. 10, p. 3194, 2018.

[4] S. Dutta, M. Mezzavilla, R. Ford, M. Zhang, S. Rangan, and M. Zorzi, "MAC layer frame design for millimeter wave

cellular system," in *Proceedings of the European Conference on Networks and Communications (EuCNC)*, pp. 117–121, Athens, Greece, June 2016.

[5] C. H. Doan, S. Emami, D. A. Sobel, A. M. Niknejad, and R. W. Brodersen, "Design considerations for 60 GHz CMOS radios," *IEEE Communications Magazine*, vol. 42, no. 12, pp. 132–140, 2004.

[6] T. E. Bogale, X. Wang, and L. B. Le, "mmWave massive MIMO: a paradigm for 5G," in *mmWave Massive MIMO: A Paradigm for 5G*, S. Mumtaz, J. Rodriguez, and L. Dai, Eds., pp. 195–225, Acadamic Press, San Diego, CA, USA, 2017.

[7] Z. Qingling and J. Li, "Rain attenuation in millimeter wave ranges," in *Proceedings of the 7th International Symposium on Antennas, Propagation & EM Theory*, pp. 1–4, Guilin, China, October 2006.

[8] W. Hong, "Millimeter-wave antennas and arrays," in *Handbook of Antenna Technologies*, Z. Chen, D. Liu, H. Nakano, X. Qing, and T. Zwick, Eds., pp. 1787–1850, Springer, Singapore, 2016.

[9] A. C. F. Reniers, U. Johannsen, and A. B. Smolders, "Antenna-in-package measurements," in *Antenna-in-Package Technology and Applications*, pp. 115–145, IEEE, Piscataway, NJ, USA, 2020.

[10] P. Wang, Y. Li, L. Song, and B. Vucetic, "Multi-gigabit millimeter wave wireless communications for 5G: from fixed access to cellular networks," *IEEE Communications Magazine*, vol. 53, no. 1, pp. 168–178, 2015.

[11] T. S. Rappaport, Y. Xing, G. R. MacCartney, A. F. Molisch, E. Mellios, and J. Zhang, "Overview of millimeter wave communications for fifth-generation (5G) wireless networks-with a focus on propagation models," *IEEE Transactions on Antennas and Propagation*, vol. 65, no. 12, pp. 6213–6230, 2017.

[12] S. Ghosh and D. Sen, "An inclusive survey on array antenna design for millimeter-wave communications," *IEEE Access*, vol. 7, pp. 83137–83161, 2019.

[13] W. Hong, Z. H. Jiang, C. Yu et al., "Multibeam antenna technologies for 5G wireless communications," *IEEE Transactions on Antennas and Propagation*, vol. 65, no. 12, pp. 6231–6249, 2017.

[14] W. Hong, K.-H. Baek, and S. Ko, "Millimeter-wave 5G antennas for smartphones: overview and experimental demonstration," *IEEE Transactions on Antennas and Propagation*, vol. 65, no. 12, pp. 6250–6261, 2017.

[15] M. A. Matin, "Review on millimeter wave antennas—potential candidate for 5G enabled applications," *Advanced Electromagnetics*, vol. 5, no. 3, pp. 98–105, 016.

[16] K. Okada and J. Pang, "Millimeter-wave CMOS phased-array transceiver supporting dual-polarized MIMO for 5G NR," in *Proceedings of the IEEE Custom Integrated Circuits Conference (CICC)*, pp. 1–8, Boston, MA, USA, March 2020.

[17] D. Caratelli, M. C. Viganó, G. Toso, P. Angeletti, A. A. Shibelgut, and R. Cicchetti, "A hybrid deterministic/metaheuristic synthesis technique for non-uniformly spaced linear printed antenna arrays," *Progress In Electromagnetics Research*, vol. 142, pp. 107–121, 2013.

[18] T. S. Rappaport, S. Sun, and M. Shafi, "Investigation and comparison of 3GPP and NYUSIM channel models for 5G wireless communications," in *Proceedings of the IEEE 86th Vehicular Technology Conference (VTC-Fall)*, pp. 1–5, Toronto, ON, Canada, September 2017.

[19] T. S. Rappaport, G. R. MacCartney, M. K. Samimi, and S. Sun, "Wideband millimeter-wave propagation measurements and channel models for future wireless communication system design," *IEEE Transactions on Communications*, vol. 63, no. 9, pp. 3029–3056, 2015.

[20] D. Chizhik, J. Du, R. Feick, M. Rodriguez, G. Castro, and R. A. Valenzuela, "Path loss and directional gain measurements at 28 GHz for non-line-of-sight coverage of indoors with corridors," *IEEE Transactions on Antennas and Propagation*, vol. 68, no. 6, pp. 4820–4830, 2020.

[21] K. Bechta, J. Du, and M. Rybakowski, "Rework the radio link budget for 5G and beyond," *IEEE Access*, vol. 8, pp. 211585–211594, 2020.

[22] 3GPP Radio Access Network Working Group, *Study on Channel Model for Frequencies from 0.5 to 100 GHz (Release 15)*, 3GPP TR 38.901 V15.0.0, Sophia Antipolis, France.

[23] B. J. West, "Phased array antenna technology," in *The RF and Microwave Handbook*, M. Golio, Ed., pp. 1037–1057, CRC Press Taylor & Francis group, Inc., Boca Raton, FL, USA, 1st edition, 2001.

[24] Y. Li, S. Xiao, and J. Guo, "A review of wideband wide-angle scanning 2-D phased array and its applications in satellite communication," *Journal of Communications and Information Networks*, vol. 3, no. 1, pp. 21–30, 2018.

[25] H. Singh, H. L. Sneha, and R. M. Jha, "Mutual coupling in phased arrays: a review," *International Journal of Antennas and Propagation*, vol. 2013, Article ID 348123, 23 pages, 2013.

[26] R. Hill, "A practical guide to the design of microstrip antenna arrays," *Microwave Journal*, vol. 44, 2001.

[27] D. Caratelli, G. Toso, O. V. Stukach, and N. V. Panokin, "Deterministic constrained synthesis technique for conformal aperiodic linear antenna arrays-Part I: theory," *IEEE Transactions on Antennas and Propagation*, vol. 67, no. 9, pp. 5951–5961, 2019.

[28] D. Caratelli, G. Toso, O. V. Stukach, and N. V. Panokin, "Deterministic constrained synthesis technique for conformal aperiodic linear antenna arrays-part II: applications," *IEEE Transactions on Antennas and Propagation*, vol. 67, no. 9, pp. 5962–5973, 2019.

[29] P. J. Gibson, "The Vivaldi aerial," in *Proceedings of the 9th European Microwave Conference*, pp. 101–105, Bringhton, UK, September 1979.

[30] S. Zhu, H. Liu, Z. Chen, and P. Wen, "A compact gain-enhanced Vivaldi antenna array with suppressed mutual coupling for 5G mmWave application," *IEEE Antennas and Wireless Propagation Letters*, vol. 17, no. 5, pp. 776–779, 2018.

[31] P. Kumar, Z. Akhter, A. K. Jha, and M. J. Akhtar, "Directivity enhancement of double slot Vivaldi antenna using anisotropic zero-index metamaterials," in *Proceedings of the IEEE International Symposium on Antennas and Propagation & USNC/URSI National Radio Science Meeting*, pp. 2061-2062, Vancouver, BC, Canada, July 2015.

[32] A. Loutridis, S. Kazıcı, O. V. Stukach, A. B. Mirmanov, and D. Caratelli, "A novel class of super-elliptical Vivaldi antennas for ultra-wideband Applications," in *Advanced Radio Frequency Antennas for Modern Communication and Medical Systems*Albert Sabban, IntechOpen, London, UK, 2020.

[33] M. Moosazadeh and S. Kharkovsky, "A compact high-gain and front-to-back ratio elliptically tapered antipodal Vivaldi antenna with trapezoid-shaped dielectric lens," *IEEE Antennas and Wireless Propagation Letters*, vol. 15, pp. 552–555, 2016.

[34] P. Bia, D. Caratelli, L. Mescia, and J. Gielis, "Electromagnetic characterization of supershaped lens antennas for high-frequency applications," in *Proceedings of the European*

Radar Conference, pp. 367–370, Nuremberg, Germany, October 2013.

[35] L. Mescia, P. Bia, D. Caratelli, M. A. Chiapperino, O. Stukach, and J. Gielis, "Electromagnetic mathematical modeling of 3D supershaped dielectric lens antennas," *Mathematical Problems in Engineering*, vol. 2016, Article ID 8130160, 10 pages, 2016.

[36] H.-X. Xu, G.-M. Wang, Z. Tao, and T. J. Cui, "High-directivity emissions with flexible beam numbers and beam directions using gradient-refractive-index fractal metamaterial," *Scientific Reports*, vol. 4, no. 1, 2014.

[37] I. T. Nassar and T. M. Weller, "A novel method for improving antipodal Vivaldi antenna performance," *IEEE Transactions on Antennas and Propagation*, vol. 63, no. 7, pp. 3321–3324, 2015.

[38] R. Schulpen, U. Johannsen, S. C. Pires, and A. B. Smolders, "Design of a phased-array antenna for 5G base station applications in the 3.4–3.8 GHz band," in *Proceedings of the 12th European Conference on Antennas and Propagation (EuCAP)*, pp. 1–5, London, UK, April 2018.

[39] S. Keyrouz and D. Caratelli, "Dielectric resonator antennas: basic concepts, design guidelines, and recent developments at millimeter-wave frequencies," *International Journal of Antennas and Propagation*, vol. 2016, Article ID 6075680, 20 pages, 2016.

[40] M. Simeoni, R. Cicchetti, A. Yarovoy, and D. Caratelli, "Supershaped dielectric resonator antennas," in *Proceedings of the IEEE 2009 IEEE Antennas and Propagation Society International Symposium AP-S/URSI*, Charleston, SC, USA, June 2009.

[41] M. Simeoni, R. Cicchetti, A. Yarovoy, and D. Caratelli, "Circularly polarized supershaped dielectric resonator antennas for indoor ultra wide band applications," in *Proceedings of the 2010 IEEE Antennas and Propagation Society IEEE AP-S/URSI International Symposium*, Toronto, ON, Canada, July 2010.

[42] E. Baldazzi, A. Al-Rawi, R. Cicchetti et al., "A high-gain dielectric resonator antenna with plastic-based conical horn for millimeter-wave applications," *IEEE Antennas and Wireless Propagation Letters*, vol. 19, no. 6, p. 949, 2020.

[43] A. Petosa and A. Ittipiboon, "Dielectric resonator antennas: a historical review and the current state of the art," *IEEE Antennas and Propagation Magazine*, vol. 52, no. 5, pp. 91–116, 2010.

[44] Y. J. Cheng, K. Wu, and W. Hong, "Power handling capability of substrate integrated waveguide interconnects and related transmission line systems," *IEEE Transactions on Advanced Packaging*, vol. 31, no. 4, pp. 900–909, 2008.

[45] Y. J. Cheng, *Substrate Integrated Antennas and Arrays*, pp. 1–52, CRC Press, Boca Raton, FL, USA, 2015.

[46] T. Djerafi, A. Doghri, and K. Wu, "Substrate integrated waveguide antennas," in *Handbook of Antenna Technologies*, Z. Chen, Ed., pp. 1585–1655, Springer, Singapore, 2015.

[47] E. Rajo-Iglesias, M. Ferrando-Rocher, and A. U. Zaman, "Gap waveguide technology for millimeter-wave antenna systems," *IEEE Communications Magazine*, vol. 56, no. 7, pp. 14–20, 2018.

[48] A. U. Zaman and P. S. Kildal, "Gap waveguides," in *Handbook of Antenna Technologies*, Z. Chen, D. Liu, H. Nakano, X. Qing, and T. Zwick, Eds., pp. 3273–3347, Springer, Singapore, 2016.

[49] A. Goudarzi, M. M. Honari, and R. Mirzavand, "Resonant cavity antennas for 5G communication systems: a review," *Electronics*, vol. 9, no. 7, p. 1080, 2020.

[50] T. S. Bird, "Reflector Antennas," in *Handbook of Antenna Technologies*, Z. Chen, D. Liu, H. Nakano, X. Qing, and T. Zwick, Eds., pp. 853–922, Springer, Singapore, 2016.

[51] K. Kibaroglu, M. Sayginer, T. Phelps, and G. M. Rebeiz, "A 64-element 28-GHz phased-array transceiver with 52-dBm EIRP and 8-12-Gb/s 5G link at 300 meters without any calibration," *IEEE Transactions on Microwave Theory and Techniques*, vol. 66, no. 12, pp. 5796–5811, 2018.

[52] K. Klionovski, M. S. Sharawi, and A. Shamim, "A dual-polarization-switched beam patch antenna array for millimeter-wave applications," *IEEE Transactions on Antennas and Propagation*, vol. 67, no. 5, pp. 3510–3515, 2019.

[53] K. F. Lee and J. S. Dahele, "Characteristics of microstrip patch antennas and some methods of improving frequency agility and bandwidth," in *Handbook of Microstrip Antennas*, J. R. James and P. S. Hall, Eds., pp. 111–217, Peter Peregrinus Ltd., London, UK, 1989.

[54] H. Moody, "The systematic design of the butler matrix," *IEEE Transactions on Antennas and Propagation*, vol. 12, no. 6, pp. 786–788, 1964.

[55] K. Xiang and F. Chen, "4 × 4 broadband butler matrix and its application in antenna arrays," in *Proceedings of the IEEE International Symposium on Antennas and Propagation and USNC-URSI Radio Science Meeting*, pp. 675-676, Atlanta, GA, USA, December 2019.

[56] J. Pang, R. Wu, Y. Wang et al., "A 28-GHz CMOS phased-array transceiver based on LO phase-shifting architecture with gain invariant phase tuning for 5G new radio," *IEEE Journal of Solid-State Circuits*, vol. 54, no. 5, pp. 1228–1242, 2019.

[57] T. Sowlati, S. Sarkar, B. G. Perumana et al., "A 60-GHz 144-element phased-array transceiver for backhaul application," *IEEE Journal of Solid-State Circuits*, vol. 53, no. 12, pp. 3640–3659, 2018.

[58] Y. Développement, "5G's impact on RF front-end module and connectivity for cell phones 2019," 2021, http://www.yole.fr/yole–reports.aspx.

[59] J. D. Dunworth, A. Homayoun, B.-H. Ku et al., "A 28 GHz bulk-CMOS dual-polarization phased-array transceiver with 24 channels for 5G user and base station equipment," in *Proceedings of the IEEE International Solid-State Circuits Conference (ISSCC)*, pp. 70–72, San Francisco, CA, USA, March 2018.

[60] W. Qualcomm, "Wireless technology & innovation—mobile technology—qualcomm," 2021, https://www.qualcomm.com/.

[61] H. Kim, B.-S. Park, S.-S. Song et al., "A 28 GHz CMOS direct conversion transceiver with packaged antenna arrays for 5G cellular system," in *Proceedings of the IEEE Radio Frequency Integrated Circuits Symposium (RFIC)*, pp. 69–72, Honolulu, HI, USA, June 2017.

[62] X. Gu, D. Liu, C. Baks et al., "Development, implementation, and characterization of a 64-element dual-polarized phased-array antenna module for 28-GHz high-speed data communications," *IEEE Transactions on Microwave Theory and Techniques*, vol. 67, no. 7, pp. 2975–2984, 2019.

[63] I. Nasr, R. Jungmaier, A. Baheti et al., "A highly integrated 60 GHz 6-channel transceiver with antenna in package for smart sensing and short-range communications," *IEEE Journal of Solid-State Circuits*, vol. 51, no. 9, pp. 2066–2076, 2016.

[64] Y. Zhang, "Antenna-in-package technology: its early development (historical corner)," *IEEE Antennas and Propagation Magazine*, vol. 61, no. 3, pp. 111–118, 2019.

[65] S. Shahramian, M. J. Holyoak, A. Singh, and Y. Baeyens, "A fully integrated 384-element, 16-tile, W -band phased array with self-alignment and self-test," *IEEE Journal of Solid-State Circuits*, vol. 54, no. 9, pp. 2419–2434, 2019.

[66] N. Ojaroudiparchin, M. Shen, and G. F. Pedersen, "Design of Vivaldi antenna array with end-fire beam steering function for 5G mobile terminals," in *Proceedings of the 23rd Telecommunications Forum Telfor (TELFOR)*, pp. 587–590, Belgrade, Serbia, November 2015.

[67] S. Long, M. McAllister, and L. Liang Shen, "The resonant cylindrical dielectric cavity antenna," *IEEE Transactions on Antennas and Propagation*, vol. 31, no. 3, pp. 406–412, 1983.

[68] D. Caratelli, A. Al-Rawi, J. Song, and D. Favreau, "Dielectric resonator antenna arrays for 5G wireless communications," *Microwave Journal*, vol. 63, no. 2, pp. 36–46, 2020.

[69] C. Bencivenni, M. Gustafsson, A. Haddadi, A. U. Zaman, and T. Emanuelsson, "5G mmWave beam steering antenna development and testing," in *Proceedings of the 13th European Conference on Antennas and Propagation (EuCAP)*, pp. 1–4, Krakow, Poland, June 2019.

[70] Y. C. Mark TAN, N. G. Guan Hong, and Y. S. Roger TAY, "A 2-by-2 sub-array for scalable 28 GHz mm-wave phased array horn antenna in 5G network," in *Proceedings of the 13th European Conference on Antennas and Propagation (EuCAP)*, pp. 1–5, Krakow, Poland, June 2019.

[71] R. Budé, U. Johannsen, T. Bressner, A. B. Smolders, and M. V. Ivashina, "Sparse array topologies for 5G mmWave base-stations: a system-level study," 2020.

[72] A. B. Smolders, "Design and construction of a broadband wide-scan angle phased-array antenna with 4096 radiating elements," in *Proceedings of the International Symposium on Phased Array Systems and Technology*, pp. 87–92, Boston, MA, USA, October 1996.

[73] J. Ala-Laurinaho, J. Aurinsalo, A. Karttunen et al., "2-D beam-steerable integrated lens antenna system for 5G E -band access and backhaul," *IEEE Transactions on Microwave Theory and Techniques*, vol. 64, no. 7, pp. 2244–2255, 2016.

[74] Y. Zeng and R. Zhang, "Millimeter wave MIMO with lens antenna array: a new path division multiplexing paradigm," *IEEE Transactions on Communications*, vol. 64, no. 4, pp. 1557–1571, 2016.

[75] Y. J. Cho, G.-Y. Suk, B. Kim, D. K. Kim, and C.-B. Chae, "RF lens-embedded antenna array for mmWave MIMO: design and performance," *IEEE Communications Magazine*, vol. 56, no. 7, pp. 42–48, 2018.

[76] A. Dubok, A. Al-Rawi, N. Tessema et al., "Double-reflector configuration for optimal exposure of wideband focal-plane arrays with optical beamforming," *IEEE Transactions on Antennas and Propagation*, vol. 65, no. 8, pp. 4316–4321, 2017.

[77] A. B. Smolders, A. Dubok, N. M. Tessema et al., "Building 5G millimeter-wave wireless infrastructure: wide-scan focal-plane arrays with broadband optical beamforming," *IEEE Antennas and Propagation Magazine*, vol. 61, no. 2, pp. 53–62, 2019.

[78] S. Costanzo, F. Venneri, A. Borgia, and G. D. Massa, "Dual-band dual-linear polarization reflectarray for mmWaves/5G applications," *IEEE Access*, vol. 8, pp. 78183–78192, 2020.

[79] Y.-X. Sun and K. W. Leung, "Millimeter-wave substrate-based dielectric reflectarray," *IEEE Antennas and Wireless Propagation Letters*, vol. 17, no. 12, pp. 2329–2333, 2018.

[80] Y. Liu, Y. J. Cheng, X. Y. Lei, and P. F. Kou, "Millimeter-wave single-layer wideband high-gain reflectarray antenna with

ability of spatial dispersion compensation," *IEEE Transactions on Antennas and Propagation*, vol. 66, no. 12, pp. 6862–6868, 2018.

[81] M. Akbari, S. Gupta, R. Movahedinia, S. Zarbakhsh, and A. R. Sebak, "Bandwidth enhancement of 4 × 4 subarrays circularly polarized rectangular dielectric resonator antenna by sequential feeding network," in *Proceedings of the 10th European Conference on Antennas and Propagation (EuCAP)*, pp. 1–4, Davos, Switzerland, April 2016.

[82] S.-L. S. Yang, R. Chair, A. A. Kishk, K.-F. Lee, and K.-M. Luk, "Study on sequential feeding networks for subarrays of circularly polarized elliptical dielectric resonator antenna," *IEEE Transactions on Antennas and Propagation*, vol. 55, no. 2, pp. 321–333, 2007.

[83] W. Mazhar, D. M. Klymyshyn, G. Wells, A. A. Qureshi, M. Jacobs, and S. Achenbach, "Low-profile Artificial grid dielectric resonator antenna arrays for mm-wave applications," *IEEE Transactions on Antennas and Propagation*, vol. 67, no. 7, pp. 4406–4417, 2019.

[84] W. Mazhar, D. Klymyshyn, G. Wells, A. Qureshi, and M. Jacobs, "60 GHz substrate integrated waveguide-fed monolithic grid dielectric resonator antenna arrays," *IEEE Antennas and Wireless Propagation Letters*, vol. 18, no. 6, pp. 1109–1113, 2019.

[85] Y. Li, "A *Ka*-band 3D printed horn antenna array," in *Proceedings of the International Conference on Microwave and Millimeter Wave Technology (ICMMT), Technology (ICMMT)*, pp. 1–3, Guangzhou, China, May 2019.

[86] W. T. Sethi, M. A. Ashraf, A. Ragheb, A. Alasaad, and S. A. Alshebeili, "Demonstration of millimeter wave 5G setup employing high-gain Vivaldi array," *International Journal of Antennas and Propagation*, vol. 2018, Article ID 3927153, 12 pages, 2018.

[87] Y. Cai, Z. Qian, Y. Zhang, J. Jin, and W. Cao, "Bandwidth enhancement of SIW horn antenna loaded with air-via perforated dielectric slab," *IEEE Antennas and Wireless Propagation Letters*, vol. 13, pp. 571–574, 2014.

[88] Z. Qi, X. Li, J. Xiao, and H. Zhu, "Dielectric-slab-loaded hollow substrate-integrated waveguide *H*-plane horn antenna array at *Ka*-band," *IEEE Antennas and Wireless Propagation Letters*, vol. 18, no. 9, pp. 1751–1755, 2019.

[89] H. Wang, D. Fang, B. Zhang, and W. Che, "Dielectric loaded substrate integrated waveguide (SIW) H-plane horn antennas," *IEEE Transactions on Antennas and Propagation*, vol. 58, no. 3, pp. 640–647, 2010.

[90] H. Xu, J. Zhou, K. Zhou, Q. Wu, Z. Yu, and W. Hong, "Planar wideband circularly polarized cavity-backed stacked patch antenna array for millimeter-wave applications," *IEEE Transactions on Antennas and Propagation*, vol. 66, no. 10, pp. 5170–5179, 2018.

[91] L. Qin, Y. Lu, Q. You, Y. Wang, J. Huang, and P. Gardner, "Millimeter-wave slotted waveguide array with unequal beamwidths and low sidelobe levels for vehicle radars and communications," *IEEE Transactions on Vehicular Technology*, vol. 67, no. 11, pp. 10574–10582, 2018.

[92] A. U. Zaman and P. Kildal, "Different gap waveguide slot array configurations for mmwave fixed beam antenna application," in *Proceedings of the 10th European Conference on Antennas and Propagation (EuCAP)*, pp. 1–4, Davos, Switzerland, 2016.

[93] N. Hussain, M.-J. Jeong, J. Park, and N. Kim, "A broadband circularly polarized fabry-perot resonant antenna using A single-layered PRS for 5G MIMO applications," *IEEE Access*, vol. 7, pp. 42897–42907, 2019.

[94] B. Thors, A. Furuskär, D. Colombi, and C. Törnevik, "Time-averaged realistic maximum power levels for the assessment of radio frequency exposure for 5G radio base stations using massive MIMO," *IEEE Access*, vol. 5, pp. 19711–19719, 2017.

[95] N. Ojaroudiparchin, M. Shen, and G. F. Pedersen, "8 × 8 planar phased array antenna with high efficiency and insensitivity properties for 5G mobile base stations," in *Proceedings of the 10th European Conference on Antennas and Propagation (EuCAP)*, pp. 1–5, Davos, Switzerland, April 2016.

[96] A. Dadgarpour, A. A. Kishk, and T. A. Denidni, "Gain enhancement of planar antenna enabled by array of split-ring resonators," *IEEE Transactions on Antennas and Propagation*, vol. 64, no. 8, pp. 3682–3687, 2016.

[97] M. Asaadi and A. Sebak, "Gain and bandwidth enhancement of 2 × 2 square dense dielectric patch antenna array using a holey superstrate," *IEEE Antennas and Wireless Propagation Letters*, vol. 16, pp. 1808–1811, 2017.

[98] X. Zhang and L. Zhu, "Gain-enhanced patch antenna without enlarged size via loading of slot and shorting pins," *IEEE Transactions on Antennas and Propagation*, vol. 65, no. 11, pp. 5702–5709, 2017.

[99] W. E. McKinzie, D. M. Nair, B. A. Thrasher, M. A. Smith, E. D. Hughes, and J. M. Parisi, "60-GHz LTCC patch antenna array with an integrated EBG structure for gain enhancement," *IEEE Antennas and Wireless Propagation Letters*, vol. 15, pp. 1522–1525, 2016.

[100] J. Coonrod, "Choosing circuit materials for millimeter wave applications," *High Frequency Electronics*, vol. 12, pp. 22–30, 2013.

[101] T. Jariyanorawiss and C. Thumkanon, "Optimization of coating material selection using the skin depth approximation," in *Proceedings of the 2018 IEEE International WIE Conference on Electrical and Computer Engineering (WIE-CON-ECE)*, pp. 114–117, Chonburi, Thailand, October 2018.

[102] A. F. Horn, J. W. Reynolds, and J. C. Rautio, "Conductor profile effects on the propagation constant of microstrip transmission lines," in *Proceedings of the IEEE MTT-S International Microwave Symposium*, pp. 868–871, Anaheim, CA, USA, June 2010.

[103] J. R. Baker-Jarvis, M. D. Janezic, B. F. Riddle, C. L. Holloway, N. G. Paulter Jr., and J. Blendell, *Dielectric and Conductor-Loss Characterization and Measurements on Electronic Packaging Materials*, NIST National Institute Standards Technology, Gaithersburg, MD, USA, 2001.

[104] D. Pozar, "Considerations for millimeter wave printed antennas," *IEEE Transactions on Antennas and Propagation*, vol. 31, no. 5, pp. 740–747, 1983.

[105] Y. Aslan, J. Puskely, J. H. J. Janssen, M. Geurts, A. Roederer, and A. Yarovoy, "Thermal-aware synthesis of 5G base station antenna arrays: an overview and a sparsity-based approach," *IEEE Access*, vol. 6, pp. 58868–58882, 2018.